Small-ELM-regime access facilitated by new tungsten divertor on EAST

G.S. Xu[1], X. Lin[1], Q. Q. Yang[1], Y. F. Wang[1], G. Z. Jia[1], N. M. Li[2], N. Yan[1], R. Chen[1], X. Q. Xu[2], H. Y. Guo[3], L. Wang[1], Q. Zang[1], T. Zhang[1], Y. F. Jin[1], B. N. Wan[1]

[1] *Institute of Plasma Physics, Chinese Academy of Sciences, Hefei 230031, China*

[2] *Lawrence Livermore National Laboratory, Livermore, CA 94550, United States of America*

[3] *Energy Singularity, Shanghai 201821, China*

A major challenge in tokamak fusion energy development is the erosion of plasma-facing materials due to excessive transient heat loading from large-amplitude edge-localized modes (ELMs). One of the most promising solutions for the excessive transient heat load is the natural small/no ELM regimes such as grassy ELM [1]. Recent studies indicate that a low pedestal density gradient is a key for access to small-ELM regimes and a wide pedestal can lead to ELM suppression [1-3]. An effective control method is required to reduce the pedestal density gradient and expand the pedestal width actively.

EAST tokamak has recently installed a new actively cooled tungsten lower divertor with the outer target plates forming a right-angled closed corner, allowing for the outer strike point being placed on either the vertical or horizontal target plate [4], as shown in Fig. 1(d). Such a divertor structure provides a new way for ELM mitigation through reducing the pedestal density gradient by controlling divertor recycling and pedestal fueling.

The three H-mode shots with the same plasma parameter settings except the lower divertor strike point position are shown in Fig 1. The plasmas are achieved at I_p = 500 kA, $B_t \sim 2.42$ T in the favorable B_t direction, $q_{95} \sim 5.6$, $\beta_p \sim 1.4$, under the lower single null (LSN)
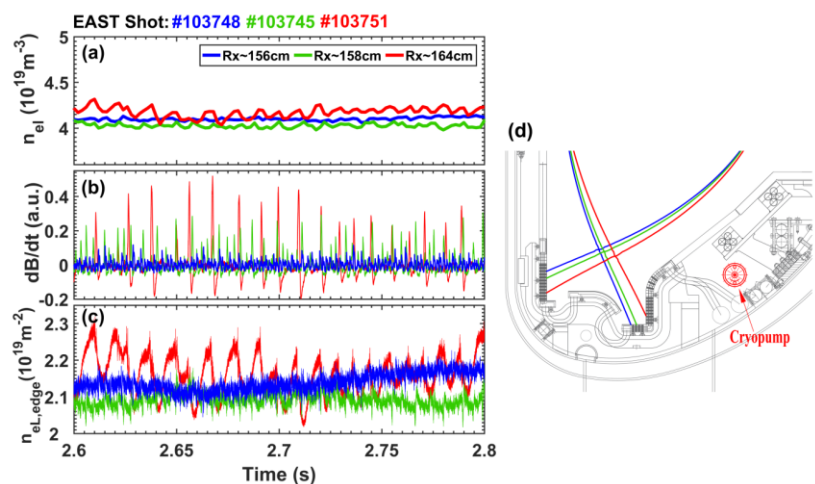

FIG. 1. Large ELMs are obtained with the strike point on the vertical target for EAST shot #103751; small ELMs and even smaller ELMs are obtained with the strike point on the horizontal target for shot #103745 and #103748.

divertor configuration with $dR_{sep} \sim 2.3$ cm. The total heating power is 3.4 MW, including 1.4 MW lower hybrid current drive (LHCD) at 4.6 GHz, 1 MW electron cyclotron resonance heating (ECRH), and 1 MW neutral beam injection (NBI). The plasma density is $n_{el} \sim 4.2 \times 10^{19}$

m^{-3}, for all the cases [Fig. 1(a)]. The movement of the divertor strike points is achieved through the feedback control of the lower X-point position by using the plasma control system (PCS) while keeping the other control points on the magnetic separatrix fixed. Large-amplitude ELMs are obtained when the outer strike point is located on the vertical target in shot #103751 with the major radius of the lower X-point, R$_x$, at ~164 cm. The ELM size appears to be significantly reduced when the outer strike point is located on the horizontal target in shot #103745 with R$_x$ ~158 cm, and even further reduced as the outer strike point is placed further away from the corner in shot #103748 with R$_x$ ~156 cm. The ELM frequency increases from f_{ELM} ~120 Hz to ~300 Hz and further to ~500 Hz, which is in a typical frequency range of small grassy ELMs. This ELM mitigation effect appears to be insensitive to q_{95} in contrast to RMPs, and has been observed in a q_{95} range of 5.3-6.4 with I_p = 450-550 kA, for both B_t directions and different heating power levels. The energy confinement is maintained in most cases with H$_{98y2}$ ≥ 1.

The pedestal profiles exhibit a dramatic change in n_e but little change in T_e, as shown in Fig 2. The change in pedestal pressure profile is mainly induced by the density profile change. When the strike point is located on the vertical target, a steep pedestal density profile, a low separatrix density and a low density ratio between the pedestal foot (separatrix) and top, $n_{e,sep}/n_{e,ped}$ ~ 0.38, are obtained. In contrast, when the strike point is located on the horizontal target, the pedestal
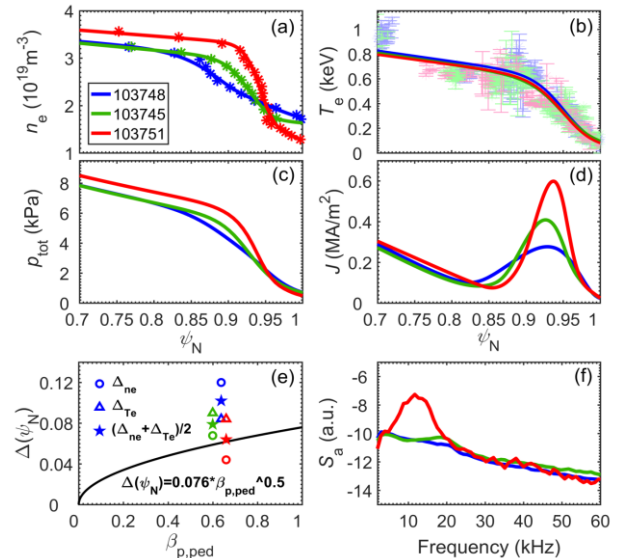

FIG. 2. Pedestal profiles for (a) n_e, (b) T_e, (c) p_{tot}, (d) J, (e) pedestal width and (f) pedestal fluctuation.

density gradient is significantly reduced with a much higher separatrix density and $n_{e,sep}/n_{e,ped}$ ~ 0.53. In particular, when the strike point is further away from the corner, an even flatter density profile is obtained with a high density ratio $n_{e,sep}/n_{e,ped}$ ~ 0.55. The pedestal width of density and pressure profiles appears to be extended with the strike point on the horizontal target. The pressure pedestal width in the vertical target case is very close to the EPED1 model prediction as shown in Fig. 2(e). As a result of the reduced gradients, a significantly lower bootstrap current density is obtained in the pedestal. This could be the main reason for the mitigation of large ELMs, as the pedestal bootstrap current is the main drive of the peeling modes and large ELMs [5]. This relationship between the appearance of a small-ELM regime and the flattening of the pedestal profiles is consistent with the EAST previous studies with the upper tungsten

divertor [1, 2] and DIII-D results [6, 7]. In addition, the disappearance of the ECM in the horizontal target case [Fig.2(f)] is consistent with the reduced pedestal pressure gradient, suggesting that the fluctuation-driven transport is not responsible for the reduced density and pressure gradients in this case.

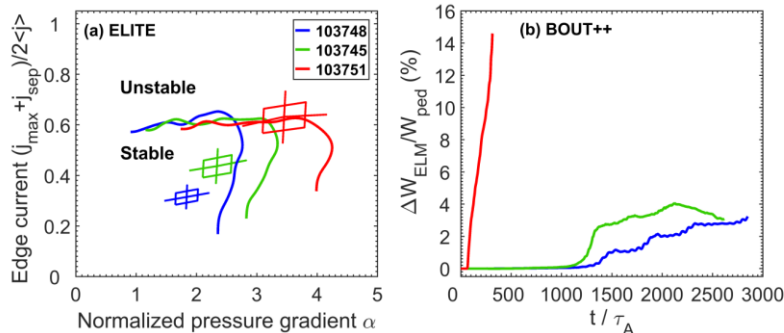The pedestal stability analysis indicate that the operational point is located right on the peeling boundary and close to the corner of the stability boundary for large ELMs with the strike point on the vertical target [Fig. 3(a)]. In contrast, the operational point is away from the peeling boundary and in the

FIG. 3. (a) Pedestal peeling-ballooning stability diagram and (b) the ELM energy loss fraction ($\Delta W_{ELM}/W_{ped}$) in the BOUT++ nonlinear simulation.

stable region for small ELMs with the strike point on the horizontal target due to reduced pedestal pressure gradient and bootstrap current density, similar to the DIII-D natural grassy ELM regime [7]. The ballooning boundary appears to shrink significantly, as a result of the reduced pressure gradient and diamagnetic frequency as they both decrease with decreasing density gradient. The lower pedestal diamagnetic frequency weakens the diamagnetic stabilization effect of the high-n ballooning modes thus helps to generate small ELMs.

In the BOUT++ simulations, the ELM energy loss with strike point on the vertical target appears to be much larger than the two horizontal target cases, consistent with the experimental observations. The simulations suggest that small ELMs can still be driven even though the ELITE linear analysis shows that they are in the stable region, which are mainly triggered by high-n ballooning modes. The effect of triangularity change on the ELM size and pedestal stability has been examined in both experiments and simulations, demonstrating that the ELM behavior change is largely due to the change in the pedestal profiles instead of the triangularity.

To uncover the mechanism of the edge density profile change for the different divertor strike point locations, SOLPS-ITER simulations with full drift effects have been performed, as illustrated in Fig. 4. The results indicate that when the strike point is located on the horizontal target, especially away from the corner, the ionization source appears to concentrate in the vicinity of the horizontal target [Figs. 4(a) & (b)] due to the trapping of the recycled particles near the closed corner. Most particles from the upstream SOL flow into the outer divertor slot and hit the horizontal target plate. Only a small number of particles in the far SOL hit the divertor baffle area, thus the recycling from the outer baffle area is very little. In addition, as the horizontal target is far away from the X-point relative to the vertical target, the recycled

particles have to travel a long distance until they reach the X-point area, thus much less recycled particles from the lower divertor are able to penetrate into the pedestal and contribute to the ionization source there. Hence, a lower pedestal density gradient and a higher density in the SOL are produced for the horizontal target cases [Fig. 4(f)]. In contrast, when the strike point is located on the vertical target, a much stronger ionization source appears in the vicinity of the X-point, especially inside the separatrix [Fig. 4(c)]. The vertical target plate reflects recycled neutral particles towards the private region where the electron density and temperature are much lower than the SOL. Therefore, the neutrals cannot be fully re-ionized in the vicinity of the X-point and tend to diffuse into the pedestal. Furthermore, as the baffle area is closer to the divertor strike point for the vertical target case, much more particles from the upstream SOL hit the baffle, which also enhance the pedestal fueling. This results in a much steeper density gradient and a lower density in the SOL for the strike point on the vertical target [Fig. 4(f)]. The radial profiles of flux-surface averaged ionization sources indicate that the ionization source in the two horizontal target cases is much lower in the pedestal but higher in the far SOL than that in the vertical target case [Fig. 4(d)], which clearly demonstrates that the difference in the ionization source associated with the divertor recycling is the dominant drive for the difference in the pedestal density profile. This difference in the flux-surface averaged ionization sources is mainly induced by the recycling in the divertor area, not from the upstream SOL, as indicated by the ionization source profile in the vicinity of X-point [Fig. 4(e)].
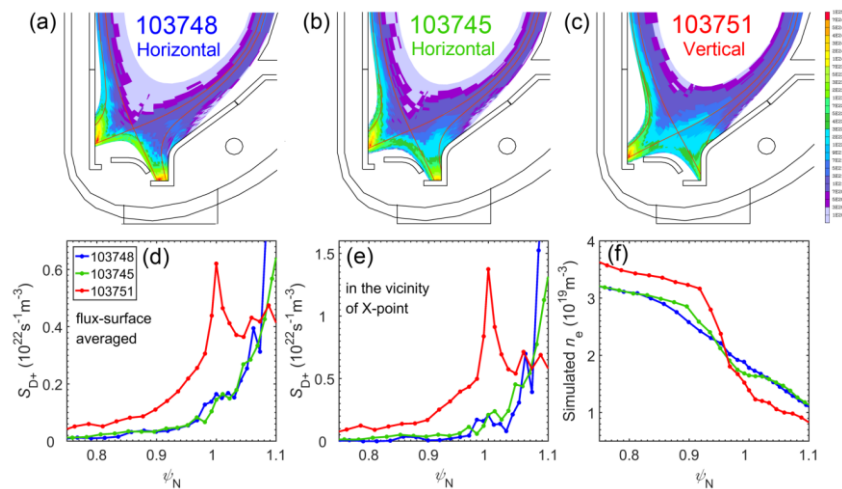

FIG. 4. SOLPS-ITER simulation results for the 3 different divertor strike point locations with full drift effects.

Reference

[1] G. S. Xu *et al.*, Phys. Rev. Lett. **122**, 255001 (2019).

[2] X. Lin *et al.*, Phys. Lett. A **431**, 127988 (2022).

[3] R. Maingi *et al.*, Phys. Rev. Lett. **107**, 145004 (2011).

[4] G. S. Xu *et al.*, Nuclear Fusion **61**, 126070 (2021).

[5] P. B. Snyder *et al.*, Physics of Plasmas **9**, 2037 (2002).

[6] R. Nazikian *et al.*, Nuclear Fusion **58**, 106010 (2018).

[7] Y. F. Wang *et al.*, Nuclear Fusion **61**, 016032 (2020).